Automatic alignment of an orbital angular momentum sorter in a transmission electron microscope using a convolution neural network

P. Rosi[1,2], A. Clausen[3], D. Weber[3], A.H. Tavabi[3], S. Frabboni[1,2], P. Tiemeijer[4], R.E. Dunin-Borkowski[3], E. Rotunno[1,*], V. Grillo[1]

1) *Istituto Nanoscienze - CNR, via G. Campi 213/A, 41125 Modena, Italy*
2) *FIM Department, University of Modena and Reggio Emilia, via G. Campi 213/A, 41125 Modena, Italy*
3) *Ernst Ruska-Centre for Microscopy and Spectroscopy with Electrons, Forschungszentrum Jülich, 52425 Jülich, Germany*
4) *Thermo Fisher Scientific, PO Box 80066, 5600 KA Eindhoven, The Netherlands*

*corresponding author address: *enzo.rotunno@nano.cnr.it*

Abstract

We report on the automatic alignment of a transmission electron microscope equipped with an orbital angular momentum sorter using a convolutional neural network. The neural network is able to control all relevant parameters of both the electron-optical setup of the microscope and the external voltage source of the sorter without input from the user. It can compensate for mechanical and optical misalignments of the sorter, in order to optimize its spectral resolution. The alignment is completed over a few frames and can be kept stable by making use of the fast fitting time of the neural network.

1-Introduction

Ever since the first electron microscope was built by Knoll and Ruska (Knoll & Ruska, 1932; Ruska, 1987), transmission electron microscopes (TEMs) have evolved considerably. Even in their simpler realizations, they contain at least 10 lenses, 3 or more detectors and several apertures, which may be motorized. However, microscope alignment, which is required at the beginning of each experimental session, is still carried out primarily by the operator using the instrument control software. Furthermore, the advances that have resulted from the introduction of spherical aberration correctors (Maximilian Haider et al., 1998; M. Haider et al., 1998; Krivanek et al., 1999), chromatic aberration correctors (Haider et al., 2008; Kabius et al., 2009) and monochromators (Tiemeijer, 1999; Krivanek et al., 2014; Morishita et al., 2016; Lopatin et al., 2018), which led to sub-atomic-resolution imaging, have further increased the complexity of such instruments. Their performance therefore still relies on the operators, making their skills a key factor during experiments. Beside the instrument itself, experiments are also becoming more complex, demanding a high level of understanding and control of the system. An example of this challenge is illustrated by electron beam shaping, a rapidly advancing field in electron microscopy that aims to provide control over the electron beam wave function using amplitude or phase plates. These amplitude or phase plates are normally fabricated using material-based holograms (Béché et al., 2014; Grillo et al., 2014, 2015; Mafakheri et al., 2017; Béché et al., 2017), but in recent years microelectromechanical systems technology (MEMS)(Verbeeck et al., 2018; Thakkar et al., 2020; Tavabi et al., 2020, 2021) has been used. The latter devices can contain electrostatic elements such as needles, toroids or spirals, whose electric fields directly affect the electrons in the beam. By using a suitable distribution of electrostatic elements and stacking multiple phase plates, it is possible to impart almost any desired phase distribution to an electron beam (Ruffato et al., 2021). An advantage of using MEMS technology is the ability to change the strength of each electrostatic element *in operando*, in effect creating a programmable phase plate. Such concepts are often inspired by light optics, where their implementation is easier and more reliable, for example by using

spatial light modulators. Recent developments in programmable structured light sources using molecular arrays (Coles et al., 2013) and plasmonic metasurfaces (Karimi et al., 2014; Pu et al., 2015) are further promoting the concept of tailored illumination. MEMS technology promises to make such concepts viable and accessible in electron microscopy, albeit at the cost of system complexity.

The complexity of electron columns and novel experimental setups is resulting in an ever higher demand for automation and instrument control, which is crucial to increase the speed, efficiency and reproducibility of electron optical alignment and to reduce the demand on the operator. Aberration correctors are currently controlled using semi-analytical models (Zemlin et al., 1978; Dellby et al., 2001; Sawada et al., 2008; Lupini et al., 2010). However, such models are not usually available for unconventional optics used in electron beam shaping. A more general approach is therefore required for microscope control. Recent advances in artificial intelligence (AI) in the automation field may be the answer for a general approach for experiments. They have prompted us to develop a convolution neural network (CNN) that can aid us in diagnosing an orbital angular momentum (OAM) sorter for electron vortex beams (Rotunno et al., 2021), but can be generalized for more complex systems such as full electron microscopes.

Electron vortex beams (EVBs) have phase singularities, around which the probability current density swirls. They possess OAM and can be used for contrast enhancement, to study magnetic materials and to probe the chirality of plasmons (Harris et al., 2015; McMorran, Agrawal, et al., 2017; Bliokh et al., 2017; Larocque et al., 2018; Shiloh et al., 2019). The generation of EVBs and the measurement of an electron beam's OAM are equally important. Although some methods can be used for both purposes (Saitoh et al., 2013; Guzzinati et al., 2014), in recent years many research groups have shifted their focus towards finding ways to measure OAM, since it provides a further parameter to characterize a specimen. Most methods provide a good estimate of OAM (Schattschneider et al., 2012; Clark et al., 2014; Verbeeck et al., 2014; Clark et al., 2016; Harvey et al., 2017; Kramberger et al., 2019; Larocque et al., 2016), but suffer from limitations since they do not decouple azimuthal and radial degrees of freedom.

An electron OAM sorter makes use of electron beam shaping to measure an electron beam's components of OAM in the propagation direction by decoupling the azimuthal and radial degrees of freedom of the electron beam. It also provides the first complete example of a lossless unitary base change that "diagonalizes" a quantum operator using wave manipulation. The implementation of an OAM sorter requires precise alignment of the electron microscope and control of two electron optical phase elements. However, no simple analytical model can be fitted to an OAM spectrum to measure the control parameters.

In this paper, we go beyond the proof of principle of our previous work by demonstrating the real time application of a neural network to control a transmission electron microscope to achieve fast, reliable and stable alignment of the OAM spectrum of an electron beam. Since a large number of electron microscope parameters have to be tuned, we anticipate that a similar approach can be used in the future to automate other measurements in the TEM, as suggested by LeBeau and colleagues (Xu et al., 2021). In light optics, there have already been several examples, both in recent years (Sorokin et al., 2020; Bhusal et al., 2021; Jin et al., 2018; Rashidi & Wolkow, 2018) and earlier (Decker, 1993), which showed how machine learning can be used for the alignment and experimental tuning of operating parameters. Just as autonomous driving has been developed thanks to artificial intelligence, it should be possible to apply similar ideas to automatic alignment in electron microscopy.

Section 2 of the present paper introduces the functioning of the OAM sorter device and the convolutional neural network that we use to tune it. As such, it summarises the content of our previous papers (Rotunno et al., 2021; Tavabi et al., 2021). In section 3, we discuss the technical details of the interface between the CNN and the microscope, which allows for automated operation of the sorting device. To the best of our knowledge, this is the first time such a level of automation has been achieved on an electron microscope. In section 4, we discuss the performance of the new self-operating setup and present future perspectives.

2- A convolutional neural network for the electron orbital angular momentum sorter

The CNN that we use to control the TEM has been designed specifically to evaluate the magnitudes of the primary parameters that need to be tuned for the alignment of an electrostatic OAM sorter [20,29]. Whereas details of the CNN are available in our previous paper [29], key elements such as the network structure and type are described below.

As a reminder, an OAM sorter is a device that is able to analyze the quantum OAM components of a vortex beam (Berkhout et al., 2010). In its most general realization, it comprises two phase-modifying elements. The first element is referred to as an unwrapper or "sorter 1" (S1), while the second element is referred to as a phase corrector or "sorter 2" (S2). The two phase elements must be in Fourier conjugate planes. The unwrapper performs a log-polar conformal transformation, which takes the azimuthal phase gradient typical of a vortex beam and converts it into a linear phase gradient. It therefore performs a conformal coordinate transformation from (x, y) to (u, v), where u and v are coordinates in the Fourier conjugate plane of the unwrapper (Berkhout et al., 2010). The phase shift introduced by the unwrapper is given by the expression

$$\varphi_{S1}(x, y) = \frac{ks}{f}\left(y \tan^{-1}\frac{y}{x} - x \log\left(\frac{\sqrt{x^2 + y^2}}{L} \right) + x \right), \tag{1}$$

where $k = \frac{1}{\lambda}$ is the electron wave vector, f is the focal distance between the sorter elements and s and L are scaling parameters. The parameter s determines the length of the transformed beam, while the parameter L translates the transformed beam along u. For an electrostatic sorter, it is defined by the length of a charged (or biased) needle that is used as the unwrapper (Berkhout et al., 2010; McMorran, Harvey, et al., 2017; Pozzi et al., 2020).

As the name suggests, the phase corrector corrects for phase inhomogeneities that are introduced by the unwrapper and prevents further S1-induced evolution of the electron beam upon propagation. Its phase shift is given by the expression

$$\varphi_{S2}(u, v) = -\frac{ksL}{f}\exp\left(-\frac{u}{s} \right)\cos\left(\frac{v}{s} \right). \tag{2}$$

We recently used MEMS technology to realize an *electrostatic* OAM sorter for electron vortex beams [20]. In this device, the unwrapper is an electrically-biased needle, while the phase corrector takes the form of a series of alternately-biased electrodes. The electrostatic potential on each needle and the electrode can be adjusted by using an external voltage source. The value of s in Eq. 1 and Eq. 2 can be changed by increasing the voltage applied to the needle in sorter 1, which increases the size of the beam in the S2 plane. The residual phase of the first element, after the transformation that it imparts to the electron beam, should then be matched perfectly by the phase of the second element. However, under the typical working conditions of the sorter, as reported in Ref.(Tavabi et al., 2021) and Ref.(Rotunno et al., 2021), the phase profiles of the elements vary rapidly in their respective planes. The alignment of the electron beam with respect to the second sorter element should therefore be nearly perfect, as a shift of only a few nm can already reduce the resolution.

As described in Ref.(Rotunno et al., 2021), the main misalignments are rotation of the unwrapped beam with respect to the phase corrector (β), size mismatch between the unwrapped beam and the periodicity of sorter 2 (SM), defocus of the beam prior to being transformed (df), incorrect positioning of the unwrapped beam in the phase corrector plane (shift X and Y) and defocus of the equivalent lens after the second sorting element. If the defocus is not corrected properly, residual curvature is present in the beam and the

phase pattern is distorted, resulting in broadening of the beam in the radial direction. The more prominent sources of loss in resolution are SM and Shift X/Y. For SM, the electron beam scale in the S2 plane is larger (smaller) than the scale dictated by the periodicity of element S2. Since the periodicity of S2 is bound to the physical distance between the electrodes and the focal distance between the two elements is fixed by the physical distance between them, SM can be corrected by changing the voltage applied to the main needle of sorter 1. An indication of SM is the presence of background fringes and a resulting loss of OAM resolution. Incorrect positioning (Shift X/Y) results in an asymmetrical background fringe pattern. In a TEM, it can be corrected easily with the beam deflectors present between the S1 and S2 planes.

The tedious and time-consuming alignments of the microscope and sorter elements that are required to obtain complete phase compensation and to optimize the sorting resolution in the final spectrum have motivated us to develop and connect a CNN to the microscope, in order to allow for fast, precise and reliable alignment.

The CNN is described in Ref.(Rotunno et al., 2021). It takes as input the image of a beam that has propagated, in vacuum, after interaction with both sorting elements, as shown in Fig 1a. The beam is a featureless, aperture-limited probe, which can be described as an $\ell = 0$ electron vortex beam and represents the point spread function (PSF) of the Sorter. As such, it is a perfect tool to characterize the performance of the sorter. The CNN itself is composed of 13 layers, as shown schematically in Figure 1: an input layer (a 128 x 128 pixel image), 5 convolution layer filters (each of which is followed by an average-pooling layer filter) and two fully connected layers leading to the output, corresponding to a total of 2,480,326 trainable parameters. The chosen activation function was the rectified linear unit (ReLU), the learning algorithm used was Adam (Kingma & Ba, 2014) and the learning rate was 0.001, while the loss function was the root mean square difference between the predicted and true misalignment coefficients. The CNN was implemented using the Keras library (Gulli & Pal, 2017) and the TensorFlow backend (Abadi et al., 2016). It was trained on a database of 20 000 images (+ 2000 images for validation) for random values of 6 misalignment parameters. The database was composed entirely of computer-generated images, making training of the CNN independent of specific hardware. Therefore, we expect the method to be reproducible on any microscope. Details of how the simulated images were obtained are reported in Ref.(Rotunno et al., 2021). It should be noted that the CNN did not converge to a correct value without accounting for decoherence, which was included by fitting a classical gaussian model directly to the experimental images (Dwyer et al., 2010; Grillo & Carlino, 2006), with different values of the coherence length used to find the correct one. The best-performing model had a gaussian width of $0.45\hbar$ in the OAM spectrum.
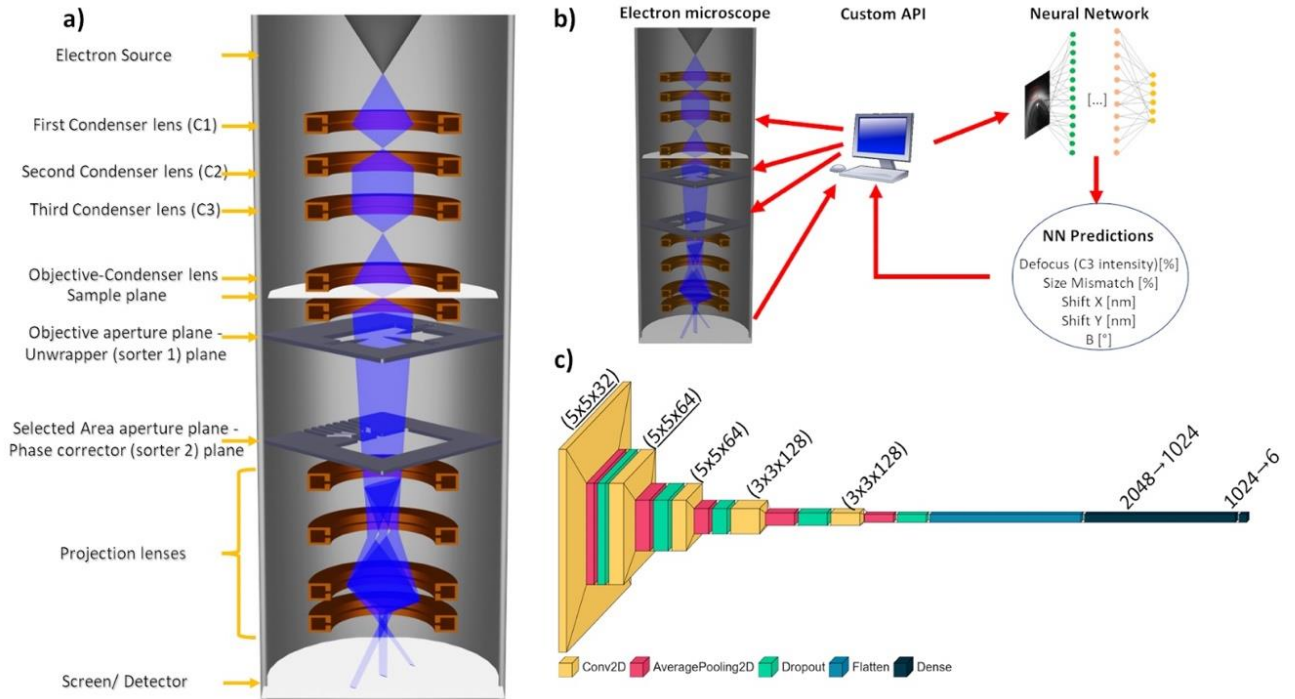
Figure 1: (a) Schematic view of a transmission electron microscope electron-optical configuration, illustrating (b) control of the TEM through the CNN, whose layout is reported in (c). Further details about the network structure can be found in Ref. [29].

3-Connecting the CNN to the microscope

In order to achieve real-time automatic alignment, image data from the microscope was fed into the CNN. Output from the CNN was converted into control commands, which were fed to the microscope and connected devices *via* application programming interfaces (APIs). The CNN and control loop run on a custom python3 script. The control loop can be described by the following steps:

1. Acquisition of an image using the K2 camera.

2. Pre-processing of the image.

3. Determination by the network of the parameters that it expects to perfectly align the sorter.

4. Application of corrections as changes to the microscope parameters and voltage sources.

3.1-Image data acquisition

Experiments were performed on an FEI Titan G2 60-300 TEM (Boothroyd et al., 2016) in Forschungszentrum Jülich. For data acquisition, a K2 camera was operated in *In Situ* (IS) mode. A prototype of a K2-IS adapter for the LiberTEM-live framework (Clausen et al., 2021) was used to perform continuous data capture and analysis at the full data rate of the K2-IS camera (400 fps at 2048 x 1860 pixels). In the present work, sets of 400 frames were summed to create 1 second exposure images at each control step. In order to work with LiberTEM-live, a processing server running the Debian GNU/Linux "Buster" distribution was connected to the data switch of the K2 camera using two 10 Gbit network interfaces. The K2 data switch was reconfigured to forward all multicast UDP datagrams coming from the K2 digitizers to the processing server. The prototype K2-IS adapter receives, decodes and sorts the UDP datagrams and executes arbitrary

processing and analysis functions (referred to as UDFs in LiberTEM) on this data stream, allowing for fast visual feedback and near-real-time feedback loops. The LiberTEM back-end and LiberTEM-live separate technical aspects, such as communication with the camera, synchronization and decoding/ re-ordering of data streams, from data processing in the UDF. In this way, a UDF can run unmodified on any data stream from a LiberTEM-compatible detector or file format.

3.2-Pre-processing

The recorded images were pre-processed to match images in the training dataset in size and orientation.

Precise calibration is crucial for the CNN to provide quantitative results. For this purpose, calibration spectra were obtained using petal beams (Tavabi et al., 2021), which have known OAM decompositions and can be produced easily using synthetic holograms made by focused ion beam milling. A review on this subject and on beam shaping using synthetic holograms is available in Ref. (Rosi et al., 2022).

Once the pixel size of the experimental images had been measured, they could be scaled, cropped and normalized over the interval [0, 1] to match the simulations in the training dataset.

As the model is not rotationally-invariant, rotation of the spectrum also had to be calibrated. Whereas the OAM axis is horizontal in the simulations, in the experimental images it is defined by the orientation of the second element of the sorter with respect to the camera and by the excitation of the lenses between them. As the OAM spectrum is dispersed along a single direction, calibration of the rotation angle is straightforward.

3.3-Inference

The network calculates the corrections that it expects to provide perfect alignment of the sorter. These settings are applied relative to the current state of the system. A damping factor and a rate limit are used to take calibration errors into account and to manage interdependence between the parameters. As demonstrated in our previous work (Rotunno et al., 2021), the network output corrections have a linear trend. Damping prevents overshooting of the target by limiting, in most cases, jumps around the convergence point. Such jumps are expected since the network was trained with limited resolution. A damping factor of 0.4 was used for the beam shift (X/Y) and intensity. A smaller damping factor of 0.2 was used for the scaling factor s of sorter S1, as it is the most sensitive parameter.

Custom calibrations were performed to provide a conversion from the damped output of the network to the units used by the microscope API. The beam shift (X/Y) had to be flipped in the X and Y directions (defined in the sorter 2 plane, where the positive direction of X moves towards S2 and Y is defined such that the right-hand rule applies), rotated (because the Cartesian coordinate system of the network is rotated with respect to the Cartesian coordinate system of the microscope) and scaled from the network output to the microscope units. The excitation values of condenser lens C3 also had to be scaled and an offset added to them. This calibration was determined by adjusting the microscope in such a way that the effect of the control inputs could be observed relative to the sorter device.

3.4-Instrument control

Multiple devices were controlled during the experiment. A 16-channel voltage source (Stahl-Electronics DC precision voltage source BS-series) was used to power the two sorter devices. The TEM parameters (beam shift (X/Y), C3 intensity and other parameters) were controlled *via* the COM scripting interface of the

microscope. All of the devices, with the exception of the K2 camera, were controlled using a Tango(Chaize et al., 2001) setup, which provides network-transparent control of different devices and encapsulates the control details in the Tango device server. After the device server was set up, it could be used by installing a Tango client library from any of the supported languages (currently LabView, Matlab/Octave, Java, Python and C++, among others) or *via* a REST API. On the client side, there are no further hardware-specific dependencies.

4-Experimental results and discussion

We performed a series of test runs using the described setup. Figure 2 shows a series of images, in which we intentionally started from an incorrect condition and the CNN was then asked to correct the OAM sorter PSF. As underlined in Section 3.1, the camera is used to perform continuous data capture to create 1 second exposure images. Only three of the main alignment parameters that act on the OAM sorter were controlled: size mismatch (*i.e.*, voltage applied to the main needle of the unwrapper) and beam shift (X/Y). As discussed above, defocus mainly results in a broadening of the beam in the radial direction and it only marginally affects the OAM resolution so it was initially neglected

In frame 000, the sorter PSF before correction is reported. It was achieved by randomly changing the controllable parameters from the final configuration achieved in the previous alignment. Due to the misalignment, the PSF is not peaked in a sharp spot corresponding to $\ell = 0$, but is broad with a diffuse background. In the labels, we reported the corrective actions proposed by the CNN. However, as mentioned before, only a fraction of it is actually applied. The effect of the correction, despite this damping, is clearly evident already in frame 001: the diffuse background is now absent, a clear fringe pattern appears instead.. Although the spectrum does not appear to be corrected from frame 001 to frame 006, close inspection indicates that the number of fringes is decreasing, with the maximum intensity jumping between two peaks until it is concentrated primarily in one peak in frame 007, with few fringes that have almost disappeared in frame 008.

It is worth noting that, after few frames, the measured beam shifts are already very low, close to the resolution limit of the CNN that we reported in our previous paper. We estimated an absolute error of 1% for the defocus and ~35 nm for the beam shifts. From frame 001 to frame 009, the SM aberration is corrected slowly due to the smaller damping factor. As a consequence of the correction, the number of fringes decreases and the central peak becomes brighter until frame 010, when the intensity is mainly concentrated in a single sharp peak with very weak lateral fringes.
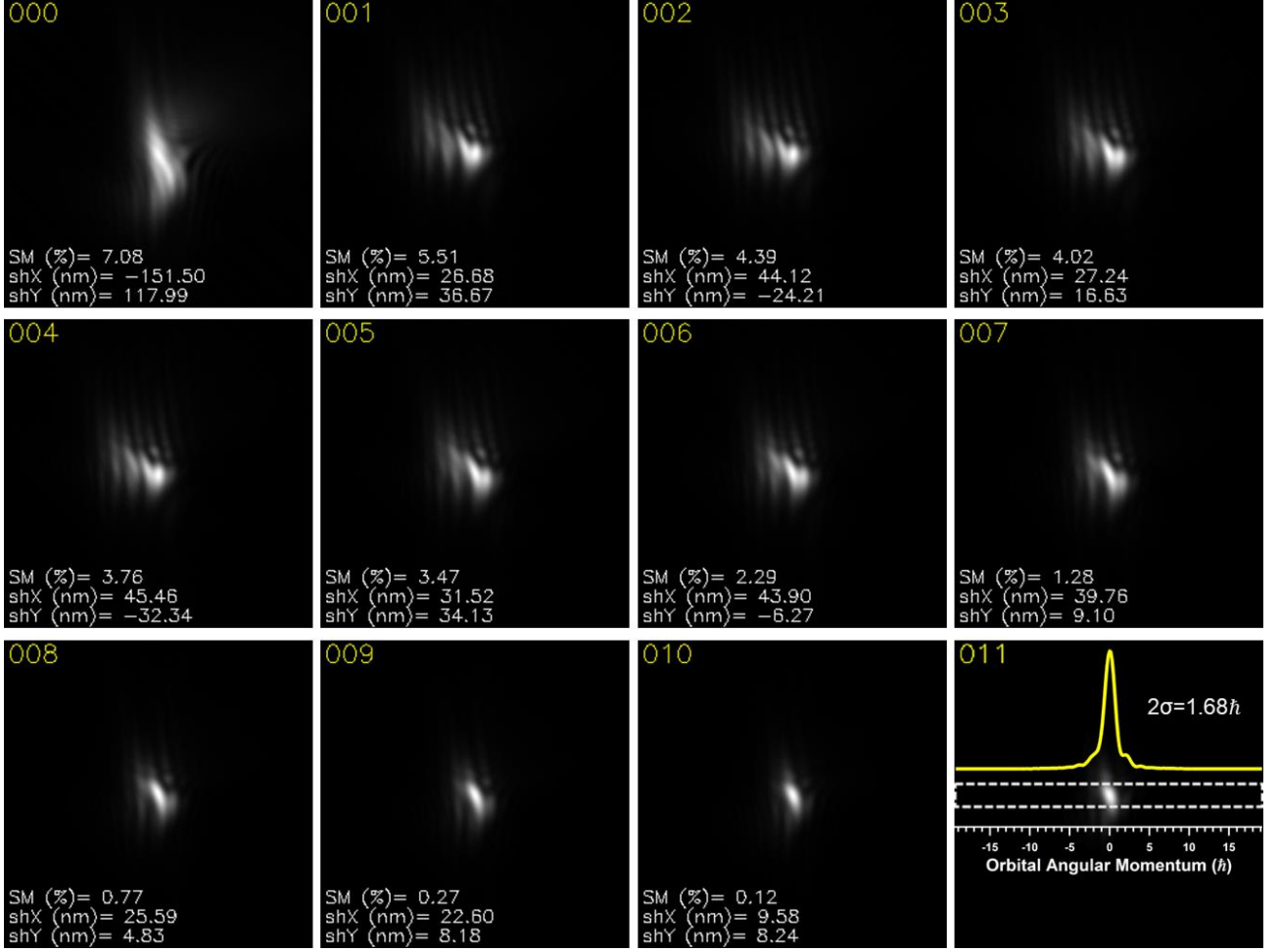
Figure 2: Experimental image series showing the evolution of an OAM spectrum of an ℓ = 0 beam (the sorter PSF) in time as the CNN provides correction values. Each image is a 1 second exposure, with the upper left corner showing the frame number (corresponding to a time stamp in seconds from frame 0) and the lower left corner showing the correctable alignment parameters estimated by the CNN, which were fed to the microscope to generate the images shown in the subsequent frames. The final frame shows in yellow an intensity profile obtained from an integrated line scan from the region marked with a dotted white line, in which the width of a gaussian profile, which corresponds to twice the standard deviation, takes a value of 1.68ℏ. The integration region is 21 pixels wide and is centered around the point of maximum intensity.

We can confirm that the CNN is working efficiently by looking at the behavior of the parameter that is commonly used to benchmark an OAM sorter: its sorting resolution. By making use of a prior pixel calibration of the OAM sorter PSF image, we systematically measured the sorting resolution in each OAM sorter PSF image. Figure 3 shows the time evolution of the sorting resolution and of the values corrected by the CNN, which were obtained by re-analysing five OAM sorter PSF image series with the same CNN that was used to control the microscope. The data denoted "series 2", with red square markers, correspond to the data shown in Fig. 2. Each of the five series shown in Fig. 3 involved starting from a random condition (by using software to randomly change the correctable parameters within the correction range after manually correcting the OAM sorter PSF), except for the starting value of the bias applied to sorter 1 (which was increased from one series to the next to see if the starting condition of sorter 1 had an effect on the final value). In each series, the sorting resolution of a randomly misaligned spectrum usually starts from a value higher than 3ℏ (except for series 4) and then quickly goes to a final average value of 1.6ℏ, in some cases even going lower and nearing our previously found OAM sorting resolution of 1.5ℏ (marked with a solid black line in the graph).

The three parameters that were corrected reached values of zero (meaning that it was not necessary to compensate for them further). This situation was achieved, on average, after 7 frames (corresponding to 7 seconds). The values then oscillated about zero, while maintaining stable spectra. For most of the series, the final stable value of the sorter 1 bias was 5.9 V, while for a couple of them it was 6.05 V, which is within the 2% tolerance that was defined in the previous paper (and therefore the degree of accuracy of the network). The sorting resolution in the five different series shown in Fig.3 improves as the three parameters are corrected, until it reaches a final value that is on average 1.6$\hbar$. Just as for the three parameters that are being corrected, the sorting resolution reaches a stable value of 1.6$\hbar$ on average after 7 iterations, i.e., 7 seconds.
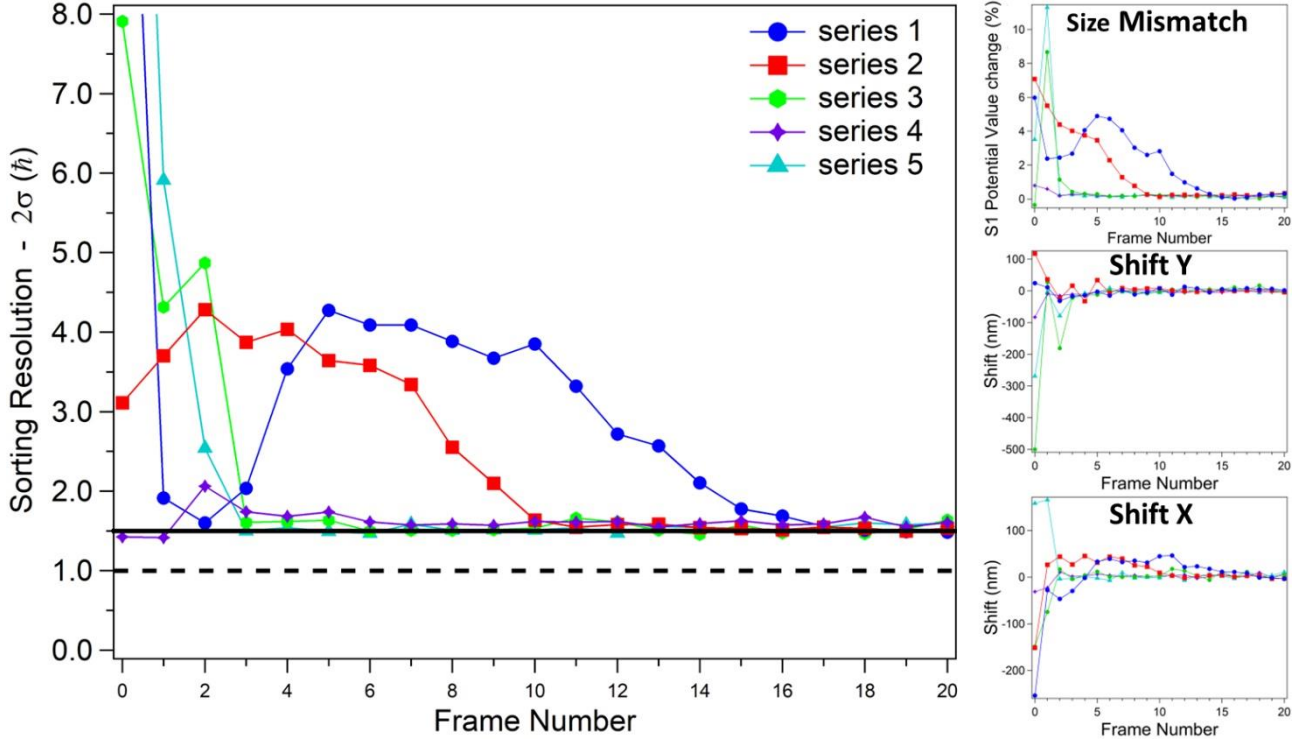

Figure 3: Behaviour of OAM sorting resolution and CNN output for different alignment series as a function of frame number, showing the size mismatch and beam shift (X/Y). The OAM sorting resolution tends to an average value of 1.6$\hbar$, while each parameter tends to zero after a few iterations. In the panel in which the trends of the sorting resolution are reported, the solid black line corresponds to the sorting resolutionthat was measured previously using manual alignment(Tavabi et al., 2021), while the dotted line represents the theoretical limit of the sorting resolution of our system.

Each additional degree of freedom managed by the CNN complicates the remote control system of the microscope. Therefore, we initially extended control over the parameters that are known to be most effective, i.e., the beam shifts and the potential applied to sorter 1 (SM in our compact notation). This level of correction gave us the 1.68$\hbar$ resolution reported in Fig. 2. Figure 3 further confirms that, by only correcting three parameters, the sorting resolution can only go down to approximately 1.6$\hbar$ This accuracy is very close to that achieved by a human operator (1.5$\hbar$ reported in Ref.(Tavabi et al., 2021)). It motivated us to increase the complexity of the control system by adding a fourth correctable parameter: the excitation of the condenser lens known as C3 (*df* in our notation), which was intentionally neglected in the first experiment due to its smaller effect on the sorting resolution. Figure 4 shows an image series that illustrates how the OAM sorter PSF is corrected and improved over time.
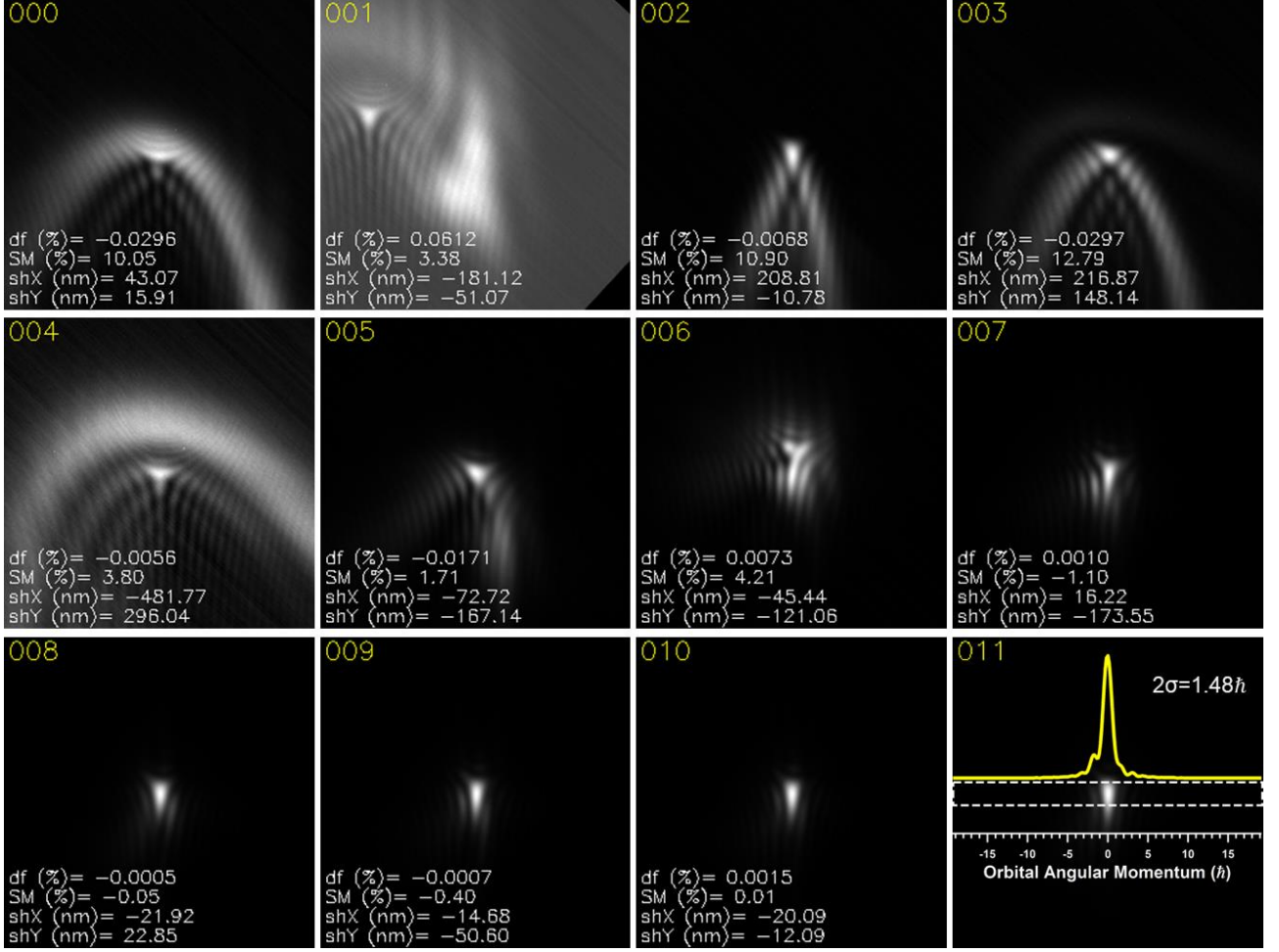
Figure 4: Experimental image series showing how the OAM sorter PSF evolves in time as the CNN provides correction values for size mismatch, beam shift (X/Y) and defocus. An initial "wrong" OAM sorter PSF was corrected by the CNN. The final frame shows (in yellow) the intensity profile obtained from an integrated linescan from the region marked with a dotted white line, in which the width of a gaussian profile, which corresponds to twice the standard deviation, takes a value of 1.48ℏ.

It is interesting to observe how robust the CNN is in Fig. 4. In the second frame, either there was a problem during image acquisition due to the beam being near to the border of the K2 sensor or the spectrum was corrected incorrectly. However, from the third frame the CNN is able to recover (even though it was fed with only partially correct data from the previous frame) and gradually compensates for the misalignments until it reaches a stable condition.

The measured sorting resolution in the final frame of Fig. 4 is determined to be approximately 1.5ℏ, which is comparable to the state-of-the-art resolution achieved by a human operator in Ref. (Tavabi et al., 2021). This is a remarkable result, since the software-guided alignment takes only a few seconds and is then able to keep this condition stable, thereby overcoming possible device or microscope instabilities. In contrast, an operator with prior experience in OAM sorter alignment usually requires several minutes to reach a comparable result, thus allowing also less experienced users to use this technology. Furthermore, conventional lens aberrations have not been considered so far, even though they also affect the resolution. Control over more TEM parameters is necessary for further improvement of the sorting resolution. Moreover, as previously mentioned, the CNN was trained on simulated images that are based upon an ideal mathematical model of the sorter, resulting in limited accuracy of the network when applied to a real situation. Refinement of the network by training it directly at the microscope using reinforcement learning

schemes is expected to reduce the number of frames that is required to tune the device. Improvements in tuning speed will allow live correction of misalignments without the user noticing the adjustments.

It should be noted that the theoretical limit of the sorter system is fixed at $1\hbar$. Considerable overlap between adjacent components is expected and can only be improved by changing the design of the two phase elements(Mirhosseini et al., 2013). Forthcoming generations of sorters will be more complicated than the present one, will offer more degrees of freedom and will consequently be harder to work with. We anticipate that the proposed automatic alignment procedure will be greatly beneficial, also in view of future developments of the technique.

5. Conclusions

In this paper, a convolutional neural network has been used to directly (i.e., without intervention of the operator) control the hardware part of the optical system of a transmission electron microscope and an external generator that controls a programmable electrostatic phase plate operated as an orbital angular momentum sorter. The neural network is robust enough to correct for misalignments that affect the experimental OAM spectrum, even though it was trained on simulated spectra. It can also be used to overcome unexpected events, such as a sudden change in defocus. Tuning of the microscope optics and external power supply takes on average less than 10 s for full correction of a spectrum, providing a final orbital angular momentum resolution of approximately $1.5\hbar$. This is a major improvement over manual correction by the microscope operator, which typically takes several minutes and requires prior experience. The neural network achieves the same resolution as that obtained by manually tuning the microscope when the same number of parameters is acted upon. The advantage is that the alignment is performed reproducibly in a few seconds, instead of the tens of minutes that are required for manual tuning. Moreover, since the OAM sorting system is not simple to tune, our automatic alignment procedure enables less experienced users to use this technology. In principle, this approach can be extended to other devices in the column, including correctors and monochromators, in the future.

Data availability statement

The data and custom API that support the findings of this study are openly available in Zenodo at http://doi.org/10.5281/zenodo.5715058 and 10.5281/zenodo.6420912, respectively.

APPENDIX

Appendix A: Settings for live processing of K2 IS data

In order to ensure proper communication and reliable data delivery, several network and Linux kernel parameters must be properly tuned:

- As the UDP datagrams are encapsulated into ethernet jumbo frames, an appropriate MTU needs to be set, for example 9000. Failure to do so will result in an increase in *rx_length_errors* statistics in the output of *ethtool -S <ifname>*;
- The UDP datagrams arrive as multiple IP fragments, which need to be assembled into whole packets by the operating system. Without adjusting the system defaults, this process may require too much memory and result in dropped frames. The available buffer memory can be changed by writing to */proc/sys/net/ipv4/ipfrag_high_thresh*. A suitable process involves the observation of assembly failures under load with *netstat -s | grep -i assem* and increasing the fragmentation threshold until they no longer appear.
- Under high load, it is possible that the UDP receives a buffer overflow, which is another possible cause of dropped packets and can be observed via netstat -s, where the "receive buffer errors" counter will increase. For the individual sockets, it can be observed by tracking the d column in *ss -unlp -m -A udp*. In order to decrease the likelihood of dropped packets, it is possible to resize the buffers by increasing */proc/sys/net/core/rmem_default* and */proc/sys/net/core/rmem_max*.
- Depending on the network hardware, it can be beneficial to set up RX (receive) queue hashing, in order to better distribute the network load across multiple CPU cores. For example, on supported network hardware, by using *ethtool -N <ifname> rx-flow-hash udp4 sdfn* the received network traffic is routed to different RX queues and therefore different CPU cores, depending on the source IP address, the destination IP address, the source port and the destination port (Herbert & de Bruijn, n.d.).

References

ABADI, M., AGARWAL, A., BARHAM, P., BREVDO, E., CHEN, Z., CITRO, C., CORRADO, G. S., DAVIS, A., DEAN, J., DEVIN, M., GHEMAWAT, S., GOODFELLOW, I., HARP, A., IRVING, G., ISARD, M., JIA, Y., JOZEFOWICZ, R., KAISER, L., KUDLUR, M., LEVENBERG, J., MANE, D., MONGA, R., MOORE, S., MURRAY, D., OLAH, C., SCHUSTER, M., SHLENS, J., STEINER, B., SUTSKEVER, I., TALWAR, K., TUCKER, P., VANHOUCKE, V., VASUDEVAN, V., VIEGAS, F., VINYALS, O., WARDEN, P., WATTENBERG, M., WICKE, M., YU, Y. & ZHENG, X. (2016). TensorFlow: Large-Scale Machine Learning on Heterogeneous Distributed Systems. http://arxiv.org/abs/1603.04467.

BÉCHÉ, A., VAN BOXEM, R., VAN TENDELOO, G. & VERBEECK, J. (2014). Magnetic monopole field exposed by electrons. *Nature Physics* **10**, 26–29. http://www.nature.com/articles/nphys2816.

BÉCHÉ, A., JUCHTMANS, R. & VERBEECK, J. (2017). Efficient creation of electron vortex beams for high resolution STEM imaging. *Ultramicroscopy* **178**, 12–19.

BERKHOUT, G. C. G., LAVERY, M. P. J., COURTIAL, J., BEIJERSBERGEN, M. W. & PADGETT, M. J. (2010). Efficient Sorting of Orbital Angular Momentum States of Light. *Physical Review Letters* **105**, 153601. https://link.aps.org/doi/10.1103/PhysRevLett.105.153601.

BHUSAL, N., LOHANI, S., YOU, C., HONG, M., FABRE, J., ZHAO, P., KNUTSON, E. M., GLASSER, R. T. & MAGAÑA-LOAIZA, O. S. (2021). Spatial Mode Correction of Single Photons Using Machine Learning. *Advanced Quantum Technologies* **4**, 2000103. https://onlinelibrary.wiley.com/doi/10.1002/qute.202000103.

BLIOKH, K. Y. Y., IVANOV, I. P. P., GUZZINATI, G., CLARK, L., VAN BOXEM, R., BÉCHÉ, A., JUCHTMANS, R., ALONSO, M. A. A., SCHATTSCHNEIDER, P., NORI, F. & VERBEECK, J. (2017). Theory and applications of free-electron vortex states. *Physics Reports* **690**, 1–70. https://linkinghub.elsevier.com/retrieve/pii/S0370157317301515.

BOOTHROYD, C., KOVÁCS, A. & TILLMANN, K. (2016). FEI Titan G2 60-300 HOLO. *Journal of large-scale research facilities JLSRF* **2**, A44. http://jlsrf.org/index.php/lsf/article/view/70.

CHAIZE, J., GOETZ, A., KLOTZ, W., MEYER, J., PEREZ, M., TAUREL, E. & VERDIER, P. (2001). The ESRF TANGO control system status. https://www.tango-controls.org/.

CLARK, L., BÉCHÉ, A., GUZZINATI, G. & VERBEECK, J. (2014). Quantitative measurement of orbital angular momentum in electron microscopy. *Physical Review A* **89**, 053818. https://link.aps.org/doi/10.1103/PhysRevA.89.053818.

CLARK, L., GUZZINATI, G., BÉCHÉ, A., LUBK, A. & VERBEECK, J. (2016). Symmetry-constrained electron vortex propagation. *Physical Review A* **93**, 063840. https://link.aps.org/doi/10.1103/PhysRevA.93.063840.

CLAUSEN, A., WEBER, D., STRAUCH, A., MÜLLER-CASPARY, K. & DUNIN-BORKOWSKI, R. E. (2021). *LiberTEM/LiberTEM-live: 0.1.0*. https://zenodo.org/record/4916316.

COLES, M. M., WILLIAMS, M. D., SAADI, K., BRADSHAW, D. S. & ANDREWS, D. L. (2013). Chiral nanoemitter array: A launchpad for optical vortices. *Laser & Photonics Reviews* **7**, 1088–1092. https://onlinelibrary.wiley.com/doi/10.1002/lpor.201300117.

DECKER, A. J. (1993). *Neural-network-directed alignment of optical systems using the laser-beam spatial filter as an example*. NASA.

DELLBY, N., KRIVANEK, O. L., NELLIST, P. D., BATSON, P. E. & LUPINI, A. R. (2001). Progress in aberration-corrected scanning transmission electron microscopy. *Microscopy* **50**, 177–185. https://academic.oup.com/jmicro/article-lookup/doi/10.1093/jmicro/50.3.177.

DWYER, C., ERNI, R. & ETHERIDGE, J. (2010). Measurement of effective source distribution and its importance for quantitative interpretation of STEM images. *Ultramicroscopy* **110**, 952–957. https://linkinghub.elsevier.com/retrieve/pii/S0304399110000100.

GRILLO, V. & CARLINO, E. (2006). A novel method for focus assessment in atomic resolution STEM HAADF experiments. *Ultramicroscopy* **106**, 603–613. https://linkinghub.elsevier.com/retrieve/pii/S0304399106000246.

GRILLO, V., KARIMI, E., BALBONI, R., GAZZADI, G. C., VENTURI, F., FRABBONI, S., PIERCE, J. S., McMORRAN, B. J. & BOYD, R. W. (2015). Electron holograms encoding amplitude and phase for the generation of arbitrary wavefunctions. *Microscopy and Microanalysis* **21**, 503–504. http://www.journals.cambridge.org/abstract_S1431927615003311.

GRILLO, V., KARIMI, E., GAZZADI, G. C., FRABBONI, S., DENNIS, M. R. & BOYD, R. W. (2014). Generation of Nondiffracting Electron Bessel Beams. *Physical Review X* **4**, 011013. https://link.aps.org/doi/10.1103/PhysRevX.4.011013.

GULLI, A. & PAL, S. (2017). *Deep Learning with Keras*. Packt Publishing Ltd.

GUZZINATI, G., CLARK, L., BÉCHÉ, A. & VERBEECK, J. (2014). Measuring the orbital angular momentum of electron beams. *Physical Review A* **89**, 025803. https://link.aps.org/doi/10.1103/PhysRevA.89.025803.

HAIDER, M., MÜLLER, H., UHLEMANN, S., ZACH, J., LOEBAU, U. & HOESCHEN, R. (2008). Prerequisites for a Cc/Cs-corrected ultrahigh-resolution TEM. *Ultramicroscopy* **108**, 167–178. https://linkinghub.elsevier.com/retrieve/pii/S030439910700232X.

HAIDER, M., ROSE, H., UHLEMANN, S., KABIUS, B. & URBAN, K. (1998). Towards 0.1 nm resolution with the first spherically corrected transmission electron microscope. *Journal of Electron Microscopy* **47**, 395–405. https://academic.oup.com/jmicro/article-lookup/doi/10.1093/oxfordjournals.jmicro.a023610.

HAIDER, MAXIMILIAN, UHLEMANN, S., SCHWAN, E., ROSE, H., KABIUS, B. & URBAN, K. (1998). Electron microscopy image enhanced. *Nature* **392**, 768–769. http://www.nature.com/articles/33823.

HARRIS, J., GRILLO, V., MAFAKHERI, E., GAZZADI, G. C., FRABBONI, S., BOYD, R. W. & KARIMI, E. (2015). Structured quantum waves. *Nature Physics* **11**, 629–634. http://www.nature.com/articles/nphys3404.

HARVEY, T. R., GRILLO, V. & MCMORRAN, B. J. (2017). Stern-Gerlach-like approach to electron orbital angular momentum measurement. *Physical Review A* **95**, 021801. https://link.aps.org/doi/10.1103/PhysRevA.95.021801.

HERBERT, T. (GOOGLE) & DE BRUIJN, W. (GOOGLE) (n.d.). Network scaling. https://www.kernel.org/doc/Documentation/networking/scaling.txt.

JIN, Y., ZHANG, Y., HU, L., HUANG, H., XU, Q., ZHU, X., HUANG, L., ZHENG, Y., SHEN, H.-L., GONG, W. & SI, K. (2018). Machine learning guided rapid focusing with sensor-less aberration corrections. *Optics Express* **26**, 30162. https://opg.optica.org/abstract.cfm?URI=oe-26-23-30162.

KABIUS, B., HARTEL, P., HAIDER, M., MULLER, H., UHLEMANN, S., LOEBAU, U., ZACH, J. & ROSE, H. (2009). First application of Cc-corrected imaging for high-resolution and energy-filtered TEM. *Journal of Electron Microscopy* **58**, 147–155. https://academic.oup.com/jmicro/article-lookup/doi/10.1093/jmicro/dfp021.

KARIMI, E., SCHULZ, S. A., DE LEON, I., QASSIM, H., UPHAM, J. & BOYD, R. W. (2014). Generating optical orbital angular momentum at visible wavelengths using a plasmonic metasurface. *Light: Science & Applications* **3**, e167–e167. http://www.nature.com/articles/lsa201448.

KINGMA, D. P. & BA, J. (2014). Adam: A Method for Stochastic Optimization. http://arxiv.org/abs/1412.6980.

KNOLL, M. & RUSKA, E. (1932). Das elektronenmikroskop. *Zeitschrift für physik* **78**, 318–339.

KRAMBERGER, C., LÖFFLER, S., SCHACHINGER, T., HARTEL, P., ZACH, J. & SCHATTSCHNEIDER, P. (2019). π/2 mode converters and vortex generators for electrons. *Ultramicroscopy* **204**, 27–33. https://linkinghub.elsevier.com/retrieve/pii/S0304399118304029.

KRIVANEK, O. L., DELLBY, N. & LUPINI, A. R. (1999). Towards sub-Å electron beams. *Ultramicroscopy* **78**, 1–11. https://linkinghub.elsevier.com/retrieve/pii/S0304399199000133.

KRIVANEK, O. L., LOVEJOY, T. C., DELLBY, N., AOKI, T., CARPENTER, R. W., REZ, P., SOIGNARD, E., ZHU, J., BATSON, P. E., LAGOS, M. J., EGERTON, R. F. & CROZIER, P. A. (2014). Vibrational spectroscopy in the electron microscope. *Nature* **514**, 209–212. http://www.nature.com/articles/nature13870.

LAROCQUE, H., BOUCHARD, F., GRILLO, V., SIT, A., FRABBONI, S., DUNIN-BORKOWSKI, R. E., PADGETT, M. J., BOYD, R. W. & KARIMI, E. (2016). Nondestructive Measurement of Orbital Angular Momentum for an Electron Beam. *Physical Review Letters* **117**, 154801. https://link.aps.org/doi/10.1103/PhysRevLett.117.154801.

LAROCQUE, H., KAMINER, I., GRILLO, V., LEUCHS, G., PADGETT, M. J., BOYD, R. W., SEGEV, M. & KARIMI, E. (2018). 'Twisted' electrons. *Contemporary Physics* **59**, 126–144. https://www.tandfonline.com/doi/full/10.1080/00107514.2017.1418046.

LOPATIN, S., CHENG, B., LIU, W.-T., TSAI, M.-L., HE, J.-H. & CHUVILIN, A. (2018). Optimization of monochromated TEM for ultimate resolution imaging and ultrahigh resolution electron energy loss spectroscopy. *Ultramicroscopy* **184**, 109–115. https://linkinghub.elsevier.com/retrieve/pii/S0304399117302073.

LUPINI, A. R., WANG, P., NELLIST, P. D., KIRKLAND, A. I. & PENNYCOOK, S. J. (2010). Aberration measurement using the Ronchigram contrast transfer function. *Ultramicroscopy* **110**, 891–898. https://linkinghub.elsevier.com/retrieve/pii/S0304399110001142.

MAFAKHERI, E., TAVABI, A. H., LU, P.-H., BALBONI, R., VENTURI, F., MENOZZI, C., GAZZADI, G. C., FRABBONI, S., SIT, A., DUNIN-BORKOWSKI, R. E., KARIMI, E. & GRILLO, V. (2017). Realization of electron vortices with large orbital

angular momentum using miniature holograms fabricated by electron beam lithography. *Applied Physics Letters* **110**, 093113. http://aip.scitation.org/doi/10.1063/1.4977879.

McMorran, B. J., Agrawal, A., Ercius, P. A., Grillo, V., Herzing, A. A., Harvey, T. R., Linck, M. & Pierce, J. S. (2017). Origins and demonstrations of electrons with orbital angular momentum. *Philosophical Transactions of the Royal Society A: Mathematical, Physical and Engineering Sciences* **375**, 20150434. https://royalsocietypublishing.org/doi/10.1098/rsta.2015.0434.

McMorran, B. J., Harvey, T. R. & Lavery, M. P. J. J. (2017). Efficient sorting of free electron orbital angular momentum. *New Journal of Physics* **19**, 023053. https://iopscience.iop.org/article/10.1088/1367-2630/aa5f6f.

Mirhosseini, M., Malik, M., Shi, Z. & Boyd, R. W. (2013). Efficient separation of the orbital angular momentum eigenstates of light. *Nature Communications* **4**, 2781. http://www.nature.com/articles/ncomms3781.

Morishita, S., Mukai, M., Suenaga, K. & Sawada, H. (2016). Resolution enhancement in transmission electron microscopy with 60-kV monochromated electron source. *Applied Physics Letters* **108**, 013107. http://aip.scitation.org/doi/10.1063/1.4939653.

Pozzi, G., Grillo, V., Lu, P.-H., Tavabi, A. H., Karimi, E. & Dunin-Borkowski, R. E. (2020). Design of electrostatic phase elements for sorting the orbital angular momentum of electrons. *Ultramicroscopy* **208**, 112861. https://linkinghub.elsevier.com/retrieve/pii/S0304399119301950.

Pu, M., Li, Xiong, Ma, X., Wang, Y., Zhao, Z., Wang, C., Hu, C., Gao, P., Huang, C., Ren, H., Li, Xiangping, Qin, F., Yang, J., Gu, M., Hong, M. & Luo, X. (2015). Catenary optics for achromatic generation of perfect optical angular momentum. *Science Advances* **1**, e1500396. https://advances.sciencemag.org/lookup/doi/10.1126/sciadv.1500396.

Rashidi, M. & Wolkow, R. A. (2018). Autonomous Scanning Probe Microscopy in Situ Tip Conditioning through Machine Learning. *ACS Nano* **12**, 5185–5189. https://pubs.acs.org/doi/10.1021/acsnano.8b02208.

Rosi, P., Venturi, F., Medici, G., Menozzi, C., Gazzadi, G. C., Rotunno, E., Frabboni, S., Balboni, R., Rezaee, M., Tavabi, A. H., Dunin-Borkowski, R. E., Karimi, E. & Grillo, V. (2022). Theoretical and practical aspects of the design and production of synthetic holograms for transmission electron microscopy. *Journal of Applied Physics* **131**, 031101. http://arxiv.org/abs/2109.11347.

Rotunno, E., Tavabi, A. H., Rosi, P., Frabboni, S., Tiemeijer, P., Dunin-Borkowski, R. E. & Grillo, V. (2021). Alignment of electron optical beam shaping elements using a convolutional neural network. *Ultramicroscopy* **228**, 113338. https://linkinghub.elsevier.com/retrieve/pii/S0304399121001224.

Ruffato, G., Rotunno, E., Giberti, L. M. C. & Grillo, V. (2021). Arbitrary Conformal Transformations of Wave Functions. *Physical Review Applied* **10**, 1–11. https://doi.org/10.1103/PhysRevApplied.15.054028.

Ruska, E. (1987). The development of the electron microscope and of electron microscopy. *Bioscience reports* **7**, 607–629.

Saitoh, K., Hasegawa, Y., Hirakawa, K., Tanaka, N. & Uchida, M. (2013). Measuring the Orbital Angular Momentum of Electron Vortex Beams Using a Forked Grating. *Physical Review Letters* **111**, 074801. https://link.aps.org/doi/10.1103/PhysRevLett.111.074801.

Sawada, H., Sannomiya, T., Hosokawa, F., Nakamichi, T., Kaneyama, T., Tomita, T., Kondo, Y., Tanaka, T., Oshima, Y., Tanishiro, Y. & Takayanagi, K. (2008). Measurement method of aberration from Ronchigram by autocorrelation function. *Ultramicroscopy* **108**, 1467–1475. https://linkinghub.elsevier.com/retrieve/pii/S0304399108001824.

Schattschneider, P., Stöger-Pollach, M. & Verbeeck, J. (2012). Novel Vortex Generator and Mode Converter for Electron Beams. *Physical Review Letters* **109**, 084801. https://link.aps.org/doi/10.1103/PhysRevLett.109.084801.

Shiloh, R., Lu, P.-H., Remez, R., Tavabi, A. H., Pozzi, G., Dunin-Borkowski, R. E. & Arie, A. (2019). Nanostructuring of electron beams. *Physica Scripta* **94**, 034004. https://iopscience.iop.org/article/10.1088/1402-4896/aaf258.

Sorokin, D., Ulanov, A., Sazhina, E. & Lvovsky, A. (2020). Interferobot: aligning an optical interferometer by a reinforcement learning agent. *Advances in Neural Information Processing Systems* **33**, 13238–13248.

Tavabi, A. H., Larocque, H., Lu, P.-H., Duchamp, M., Grillo, V., Karimi, E., Dunin-Borkowski, R. E. & Pozzi, G. (2020). Generation of electron vortices using nonexact electric fields. *Physical Review Research* **2**,

013185. https://link.aps.org/doi/10.1103/PhysRevResearch.2.013185.

TAVABI, A. H., ROSI, P., ROTUNNO, E., RONCAGLIA, A., BELSITO, L., FRABBONI, S., POZZI, G., GAZZADI, G. C., LU, P.-H., NIJLAND, R., GHOSH, M., TIEMEIJER, P., KARIMI, E., DUNIN-BORKOWSKI, R. E. & GRILLO, V. (2021). Experimental Demonstration of an Electrostatic Orbital Angular Momentum Sorter for Electron Beams. *Physical Review Letters* **126**, 094802. https://doi.org/10.1103/PhysRevLett.126.094802.

THAKKAR, P., GUZENKO, V. A., LU, P.-H., DUNIN-BORKOWSKI, R. E., ABRAHAMS, J. P. & TSUJINO, S. (2020). Fabrication of low aspect ratio three-element Boersch phase shifters for voltage-controlled three electron beam interference. *Journal of Applied Physics* **128**, 134502. http://aip.scitation.org/doi/10.1063/5.0020383.

TIEMEIJER, P. C. (1999). Analytical electron microscopy-Operation modes of a TEM monochromator. In *Institute of Physics Conference Series* vol. 161, pp. 191–194. Bristol [England]; Boston: Adam Hilger, Ltd., c1985-.

VERBEECK, J., BÉCHÉ, A., MÜLLER-CASPARY, K., GUZZINATI, G., LUONG, M. A. & DEN HERTOG, M. (2018). Demonstration of a 2 × 2 programmable phase plate for electrons. *Ultramicroscopy* **190**, 58–65. https://linkinghub.elsevier.com/retrieve/pii/S0304399117305041.

VERBEECK, J., GUZZINATI, G., CLARK, L., JUCHTMANS, R., VAN BOXEM, R., TIAN, H., BÉCHÉ, A., LUBK, A. & VAN TENDELOO, G. (2014). Shaping electron beams for the generation of innovative measurements in the (S)TEM. *Comptes Rendus Physique* **15**, 190–199. https://linkinghub.elsevier.com/retrieve/pii/S1631070513001473.

XU, M., KUMAR, A. & LEBEAU, J. (2021). Automating Electron Microscopy through Machine Learning and USETEM. *Microscopy and Microanalysis* **27**, 2988–2989. https://www.cambridge.org/core/product/identifier/S1431927621010394/type/journal_article.

ZEMLIN, F., WEISS, K., SCHISKE, P., KUNATH, W. & HERRMANN, K.-H. (1978). Coma-free alignment of high resolution electron microscopes with the aid of optical diffractograms. *Ultramicroscopy* **3**, 49–60. https://linkinghub.elsevier.com/retrieve/pii/S0304399178800060.